On the aggregate-scale partitioning of solar radiation in Arctic sea ice during the Surface Heat Budget of the Arctic Ocean (SHEBA) field experiment

Donald K. Perovich

Engineer Research and Development Center, Cold Regions Research and Engineering Laboratory, Hanover, New Hampshire, USA

Received 29 May 2004; revised 4 September 2004; accepted 4 January 2005; published 1 March 2005.

[1] The partitioning of the incident solar irradiance among reflection to the atmosphere, absorption in the snow and ice, and transmission to the ocean is a critical component of the summer melt cycle of Arctic sea ice. Observations from a year-long field experiment (Surface Heat Budget of the Arctic Ocean (SHEBA)) showed that of the solar radiation incident between 1 April and 5 October 1998, 68% was reflected to the atmosphere, 24% was absorbed in the snow and ice, and 8% was transmitted to the ocean. The amount of energy reflected to the atmosphere was greatest in May, when the surface albedo and the incident irradiance were large. The energy absorbed in the snow and ice increased slowly in April and May in conjunction with the increase in incident solar irradiance, followed by a sharp increase in June associated with the onset of melt. In spring, virtually none of the solar energy incident on snow-covered sea ice is transmitted to the ocean compared to over 90% of that incident on leads. The energy transmitted to the ocean reached a maximum near the end of the melt season in mid-August when the albedo and ice thickness were at minima and lead and pond fractions were at maxima. While much of the solar energy transmitted to the ocean was through leads, substantial portions were also transmitted through bare ice (23%) and ponded ice (16%). During the melt season, the combined energy transmitted through bare ice and ponds was equivalent to that through leads. This marked a significant change in the interaction of solar energy with the sea ice cover, with substantial amounts of solar energy transmitted to the ocean through the thin summer ice cover of SHEBA compared to the thicker ice studied in 1975 (Arctic Ice Dynamics Joint Experiment (AIDJEX)).

Citation: Perovich, D. K. (2005), On the aggregate-scale partitioning of solar radiation in Arctic sea ice during the Surface Heat Budget of the Arctic Ocean (SHEBA) field experiment, *J. Geophys. Res.*, *110*, C03002, doi:10.1029/2004JC002512.

1. Introduction

[2] The sea ice cover of the Arctic Ocean may be both a sensitive indicator, and a potential amplifier, of climate change [*Dickinson et al.*, 1987; *Moritz et al.*, 1993; *Jin et al.*, 1994; *Rind et al.*, 1995; *Battisti et al.*, 1997]. The ice-albedo feedback is a key link in the complex and potentially powerful relationship between sea ice and climate. In the broadest sense, the ice-albedo feedback is more than the amount of sunlight reflected from the surface. It includes the partitioning of solar radiation among reflection to the atmosphere, absorption in the ice, and transmission to the ocean [*Ebert et al.*, 1995]. The summer melt cycle of Arctic sea ice is in large part governed by this partitioning. Understanding the ice-ocean-atmosphere processes that control this partitioning was one of the goals of the Surface Heat Budget of the Arctic Ocean program (SHEBA) [*Moritz et al.*, 1993; *Perovich et al.*, 1999a; *Uttal et al.*, 2002].

[3] Considerable effort has been directed toward determining the albedo, the fraction of the incident solar irradiance reflected by the surface. There have been several studies investigating the spatial variability and temporal evolution of the albedo of a sea ice cover from the surface, from aircraft, and from satellites [*Langleben*, 1971; *Grenfell and Maykut*, 1977; *Grenfell and Perovich*, 1984; *Radionov et al.*, 1997; *Hanesiak et al.*, 2001]. The evolution of albedo over an annual cycle was studied in particular detail during the year-long drift of Ice Station SHEBA [*Perovich et al.*, 2002a].

[4] While there are ample albedo measurements, there are far fewer measurements of solar radiation penetrating into and through the ice [*Grenfell and Maykut*, 1977; *Buckley and Trodahl*, 1987; *Voss and Schoonmaker*, 1992; *Perovich et al.*, 1998]. Indeed, owing to logistical and technical difficulties, there have been no extensive under-ice surveys of the light transmitted through the ice. This deficiency is compounded by the tremendous spatial and temporal variability of the ice cover (Figure 1). In spring, the surface is uniform in appearance and consists primarily of snow-covered sea

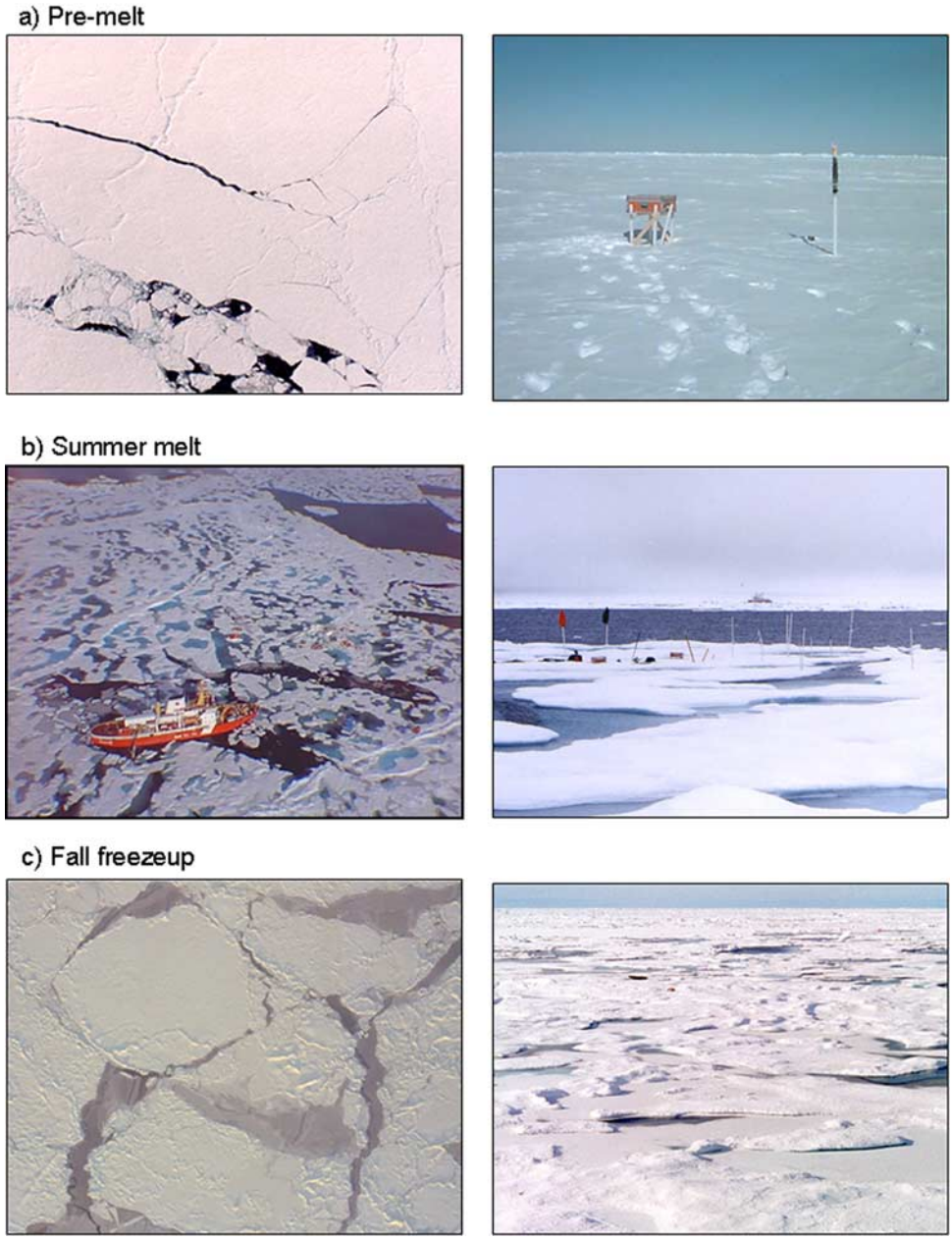

Figure 1. Surface and aerial photographs illustrating changes in ice conditions before the onset of melt in May and at the height of the melt season in August.

ice, with a small amount of open water (Figure 1a). The surface changes during the summer melt season, as it evolves into a complex, variegated mosaic of ice, ponds, and leads (Figure 1b). As fall freezeup progresses, the ponds freeze, snow falls, and the surface returns to its springtime appearance. However, there are distinct differences in the ice cover. After a summer of melting, the ice is thinner and there is more open water. In all seasons, there is considerable spatial variability in the thickness of the ice, which confounds estimating the amount of sunlight transmitted through the ice.

[5] Further complicating attempts to understand the solar partitioning are the considerable changes that appear to be occurring in the properties of the Arctic sea ice cover [*Lynch et al.*, 2001; *Vinnikov et al.*, 1999; *Serreze et al.*, 2000, 2003]. The extent of the ice cover has been steadily decreasing by 3% decade^{-1} for the past 30 years [*Parkinson et al.*, 1999; *Parkinson and Cavalieri*, 2002], the ice has been thinning [*Rothrock et al.*, 1999; *Tucker et al.*, 2001], and the amount of multiyear ice has been decreasing [*Johannessen et al.*, 1999; *Comiso*, 2002]. There is growing evidence that not only are the properties of the ice cover changing, but so are the processes governing the ice cover, including the partitioning of the solar radiation incident on the ice cover. For example, *Maykut and McPhee* [1995], analyzing results from the 1975 Arctic Ice Dynamics Joint Experiment (AIDJEX), determined that solar radiation deposited in leads was the source of the ocean heat flux. In this paper we shall examine whether or not that was also the case during the SHEBA field experiment in 1997–1998.

[6] From a climate perspective, it is important to describe the distribution of the incident solar radiation on the aggregate scale. An aggregate scale description of the ice cover is needed to link small-scale process-oriented models to large-scale climate models [*Moritz et al.*, 1993]. The term "aggregate scale" refers to the spatial scale where the sampling variability of a parameter is minimized and the observed properties of the ice pack are statistically representative. *Perovich et al.* [2002b] determined that at SHEBA this scale was approximately tens of kilometers for ice conditions, roughly the size of a grid cell in a general circulation model. *Ebert et al.* [1995] used a one-dimensional sea ice thermodynamic model and an ice thickness distribution to examine large-scale solar partitioning. However, there has not been an adequate data set to determine such a partitioning using observations. Results from the SHEBA field experiment [*Perovich et al.*, 1999a; *Uttal et al.*, 2002] provide a comprehensive, integrated data set that can be used in conjunction with a radiative transfer model to determine the temporal evolution of the distribution of solar energy. In this paper the aggregate-scale partitioning of solar radiation is examined during the period 1 April through 5 October 1998. Estimates of partitioning are generated by combining observations made during the SHEBA field experiment with a sea ice radiative transfer model. Contributions to the distribution of solar radiation by snow-covered ice, bare ice, ponded ice, and leads are computed. The total input of solar energy to the upper ocean is compared to heat consumed in melting on the underside of the ice cover.

2. Approach

[7] When considering a small homogeneous area of the ice cover, the albedo (α) is simply the fraction of the incident irradiance that is reflected, the transmittance (T) is the fraction of incident solar irradiance transmitted into the ocean, and the absorbance (B) is the fraction of incident solar irradiance absorbed in the snow and sea ice. These quantities can be measured directly or calculated using radiative transfer models. By definition, the sum of these three components is equal to 1.

[8] This equality also holds for the aggregate scale; thus

$$1 = \overline{\alpha} + \overline{T} + \overline{B},$$

where $\bar{\alpha}$, $\bar{T}$, and $\bar{B}$ are, respectively, the aggregate-scale albedo, transmittance, and absorbance. The difficulty lies in ascertaining the aggregate-scale values. This problem is ameliorated somewhat because only two of the three components need to be determined; the third is the residual. In this paper we shall determine the aggregate-scale albedo and transmittance. During SHEBA, no direct measurements were made of the aggregate scale partitioning of solar energy. However, there was a comprehensive albedo measurement program [*Perovich et al.*, 2002a] and occasional measurements of light transmission at selected sites [*Perovich et al.*, 1999b]. The albedo is strongly influenced by ice surface conditions, such as the presence of snow or water [*Grenfell and Maykut*, 1977; *Perovich*, 1996]. The aggregate-scale albedo can be estimated by combining the albedos of the various surface types present, weighted by the relative area of each type. From an albedo perspective, the sea ice cover can be simplified as a mixture of snow-covered ice, bare ice, ponded ice, and leads. The time-dependent, aggregate-scale albedo is then defined as

$$\overline{\alpha}(t) = \alpha_s(t)A_s(t) + \alpha_i(t)A_i(t) + \alpha_p(t)A_p(t) + \alpha_l(t)A_l(t), \quad (1)$$

where t is time, $\bar{\alpha}$ is the aggregate-scale albedo, α is the albedo, A is the area fraction, and the subscripts denote snow (s), bare ice (i), ponds (p), and open water (w).

[9] Unfortunately, determining the aggregate-scale transmission is far more difficult. Transmittance depends not only on the surface type, but also on the snow depth and ice thickness. There is no simple relationship to determine the amount of solar radiation transmitted to the ocean, and there is not a comprehensive set of observed transmittances. However, there was a mass balance study performed at SHEBA [*Perovich et al.*, 2003] that provides a detailed record of snow depth and ice thickness measured at more than 80 sites. These sites provided the details of the snow and ice physical properties needed for the radiative transfer model. All of these sites were snow covered in the spring, while during summer some evolved into bare ice and others into melt ponds.

[10] Results from the thickness sites were combined with a two-stream radiative transfer model to calculate the aggregate-scale transmittance [*Grenfell*, 1979; *Perovich*, 1990]. Transmittances were calculated at each gauge for each day. The individual transmittances were used to calculate average values for snow covered ice (T_s'), bare ice (T_i'), and ponded ice (T_p'). The aggregate-scale transmittance ($\overline{T}$) is calculated as

$$\overline{T}(t) = T_s'(t)A_s(t) + T_i'(t)A_i(t) + T_p'(t)A_p(t) + (1 - \alpha_l)A_l(t). \quad (2)$$

[11] The key assumption in this entire process is that the ensemble of thickness gauges are representative of the overall thickness distribution of the ice cover. In October 1997, more than 100 mass balance sites were selected to provide a representative sample of the first year, multiyear, ponded, undeformed, and deformed ice in the area around SHEBA [*Perovich et al.*, 2003]. While the representativeness of the gauges cannot be quantitatively established, it is consistent with the available information from a submarine ice thickness survey conducted at the beginning of the experiment.

[12] The solar partitioning was computed daily, even though most parameters were not measured that frequently. Incident solar irradiance was measured continuously, and daily averages were used for this study. Albedos were measured every other day, thickness measurements were made every 2–4 days, and helicopter survey flights were made irregularly. "Intelligent" linear interpolation was used to generate daily values of these parameters. For the most part, linear interpolation was used to generate parameter values for days between readings. However, daily logs were also checked for key events that would require an adjustment to linear interpolation. Such adjustments were warranted on two occasions. The logs indicated that a major divergence event in the local ice cover occurred on 31 July/1 August, implying that changes in lead fraction between

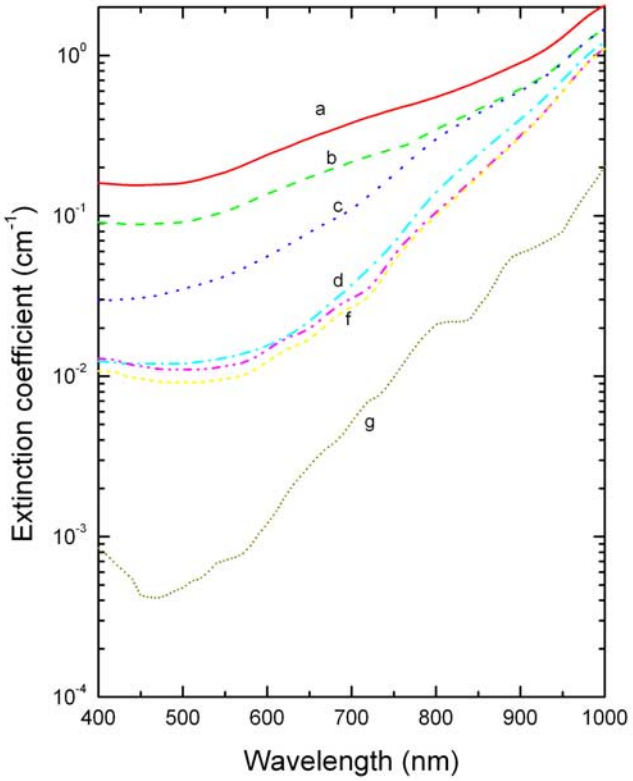

Figure 2. Spectral extinction coefficients used in the two-stream radiative transfer model. Values are plotted for (curve a) dry snow, (curve b) melting snow, (curve c) ice surface scattering layer, (curve d) drained ice, (curve e) cold ice, (curve f) melting ice, and (curve g) clear water [*Grenfell and Maykut*, 1977].

the survey flights on 25 July and 7 August were not linear. Lead fraction was assumed to be constant from 25 July to 31 July and then linearly increased from 1 August to 7 August. Intelligent interpolation was also used for determining the pond fraction during freezeup. Surface observations indicated that ponds started to freeze on 15 August. Therefore the bare ice and pond fractions observed on the 7 August survey flight were used through 15 August, followed by linear interpolation to the next survey flight datapoint on 22 August.

[13] There are numerous sea ice radiative transfer models [*Grenfell*, 1979, 1983, 1991; *Jin et al.*, 1994; *Light et al.*, 2003] of different levels of complexity that can be used to calculate transmittance. For this study, a two-stream, multilayer radiative transfer model [*Dunkle and Bevans*, 1957; *Grenfell and Maykut*, 1977] was selected. The details of the model are presented by *Perovich* [1990]. This model has the advantages of having an existing library of extinction coefficients [*Grenfell and Maykut*, 1977; *Smith and Baker*, 1981] and not requiring a detailed characterization of the physical state and structure of the snow and ice cover. It also is significantly more accurate for thinner ice than the commonly used exponential decay law [*Grenfell*, 1979]. The extinction coefficients used in this study are presented in Figure 2. A simple description of the medium suffices is as follows: dry snow (curve a) or melting snow (curve b), drained ice (curve d), cold ice (curve e) or melting ice (curve f), and surface scattering layer (curve c) or melt pond (curve g), along with the snow depth (H_s), surface scattering layer thickness (H_{ss}), ice thickness (H_i), and pond depth (H_p). Observations were used to specify the time-dependent model input for each thickness gauge. As the snow and ice properties evolved from the cold conditions of spring through summer melt into fall freezeup, the ice at the thickness gauge sites was characterized in terms of the ice types in Figure 2 and the observed thickness. April through October consisted of three periods: premelt, melt, and freezeup. Prior to the onset of melt, the ice at each gauge was assumed to consist of three layers: (1) a dry snow layer of observed depth (H_s), and (2) an upper drained ice layer equal to the freeboard ($0.1H_i$), with (3) cold ice below ($0.9H_i$). As the melt season began, the dry snow became melting snow, and the cold ice changed to melting ice. Once the snow melted, there were two ice

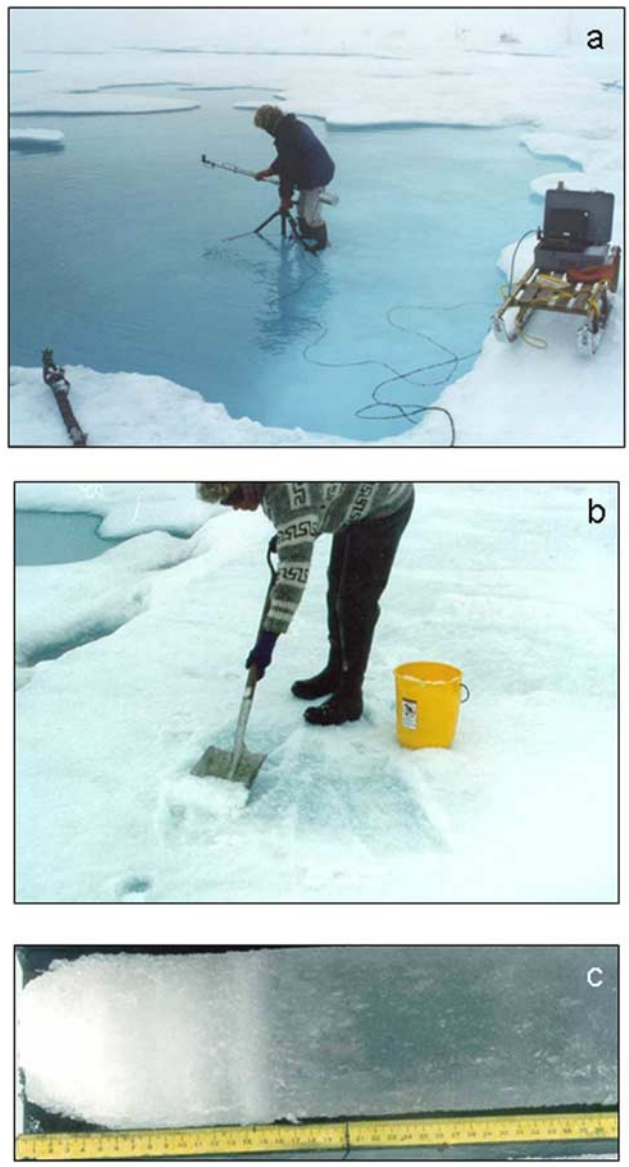

Figure 3. Melt season photographs of (a) melt pond, (b) surface scattering layer, and (c) ice core. Note the drained layer for the portion of the ice above freeboard.

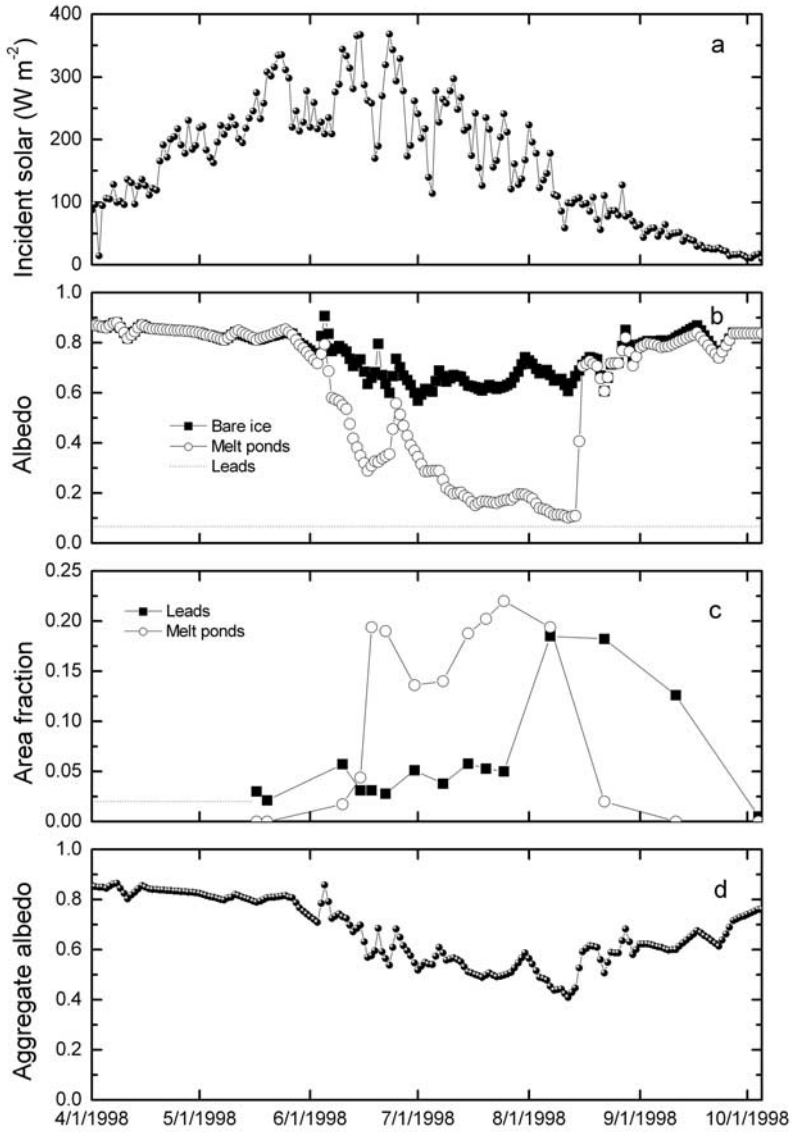

Figure 4. Time series observations measured at Ice Station SHEBA from 1 May to 5 October 1998 of (a) incident solar irradiance (R. E. Moritz, personal communication, 1999), (b) wavelength-integrated albedo [*Perovich et al.*, 2002a], (c) fractional area of ponds and leads [*Perovich et al.*, 2002b], and (d) aggregate albedo.

surface types: bare ice and ponded ice. Bare melting ice was defined to consist of three layers: (1) a surface scattering layer whose thickness was measured, (2) a drained ice layer whose thickness was equal to the ice freeboard ($0.1H_i$), and (3) melting ice ($0.9H_i$). Ponded ice consisted of clear water of observed depth (H_p), with $1.0H_i$ of melting ice underneath. During freezeup the melt pond began to freeze and new snowfall accumulated. By mid-September the surface was a mixture of snow-covered ice and open water. Model results agreed well with the few SHEBA transmittance measurements.

[14] Common ice conditions are illustrated in Figure 3, including melt ponds (Figure 3a), the surface scattering layer (Figure 3b), and a core removed from 1.5-m-thick melting ice (Figure 3c). The top 0.15 m ($0.1H_i$) of the core appears white owing to brine drainage. The remainder of the core is translucent melting ice. The surface scattering layer consisted of deteriorated, melting ice and was self-renewing throughout the melt season.

3. Results

3.1. Albedos

[15] The first step in examining the distribution of solar radiation is determining the incident solar irradiance. Daily averages of incident solar irradiance measured at Ice Station SHEBA from April through October 1998 are plotted in Figure 4a (R. E. Moritz, personal communication, 1999). The data show a general trend with an annual peak in June and a gradual decline in August and September. Superposed on this trend are short-term fluctuations of up to a factor of 2 that resulted from synoptic changes in cloud conditions. Cloudy skies were pervasive for much of July and August. While on occasion there were high-

frequency, spatial variations of incident solar irradiance (think of cloud shadowing moving across the surface) within the aggregate-scale area, daily averaged values measured at the camp are assumed to be representative of the entire area.

[16] Once the incident solar irradiance is defined, the next step is to determine the aggregate-scale albedo. Unfortunately, owing to the extensive summer cloud cover, there were only sporadic measurements of aggregate-scale albedos from either aircraft or satellites. There were, however, comprehensive surface-based measurements made of albedo [*Perovich et al.*, 2002a; *Pegau and Paulson*, 2001]. As part of this effort, albedo time series were determined for snow-covered ice, bare ice, melt ponds, and leads (Figure 4b). The pond albedo in Figure 4b is the average value, including light and dark ponds. While there were small fluctuations in lead albedo, depending on sky conditions and sun angle, lead albedos were temporally invariant on average, with a value of 0.07 [*Pegau and Paulson*, 2001]. Albedos for bare ice and ponded ice were essentially identical in spring and fall, as the ice had an optically thick snow cover. Once melt began, albedos for the bare and ponded ice diverged. Aside from a brief cold period near 20 June, pond albedos steadily decreased during the summer, while bare ice albedos varied between 0.6 and 0.7.

[17] The areal fractions of the different surface types (leads, ponds, bare ice, snow-covered ice) were determined from the analysis of photographs from survey flights [*Perovich et al.*, 2002b]. The first survey flight was on 17 May 1998. Prior to that, there were no ponds and very little open water. From 1 April to 17 May, the pond fraction was set to zero and the lead fraction was estimated as 0.02. Observations indicated that the pond fraction increased rapidly in early June and remained between 0.15 and 0.20 until freezeup in August. The amount of open water was small until 1 August 1998, when significant divergence of the ice pack near SHEBA increased the lead fraction to about 0.2. The lead fraction did not decrease until fall freezeup began a few weeks later.

[18] The albedos of individual surface types from Figure 4b and the area fractions from Figure 4c were input into equation (1) to compute the time series of aggregate-scale albedo (Figure 4d). There was a seasonal cycle of decreasing albedo during the melt season, followed by an increase associated with fall freezeup. There were several fluctuations superposed over this seasonal trend. In early summer, there were a few rapid albedo increases (6 June, 20 June, and 25 June) ascribable to brief cold periods and a dusting of snow. Around 20 June, it was cold enough that the surface of many ponds froze, causing a sharp increase in albedo. Later in the summer, from 23 to 31 July, there was a gradual, steady increase in the aggregate albedo. This resulted from a period of cooler weather that was the precursor of fall freezeup. Temperatures slightly below freezing and occasional snow flurries resulted in an increase in the bare ice albedo and the aggregate albedo. There was a sharp drop in aggregate albedo from 0.6 to 0.4 starting on 1 August. This was a direct consequence of an ice divergence event [*Richter-Menge and Perovich*, 2001] that caused a substantial increase in the lead fraction from 0.05 to 0.2. This decrease in aggregate albedo persisted until mid-August, when surface melt ended and the ponds began to freeze. By the beginning of October, aggregate albedos were only slightly less than spring values.

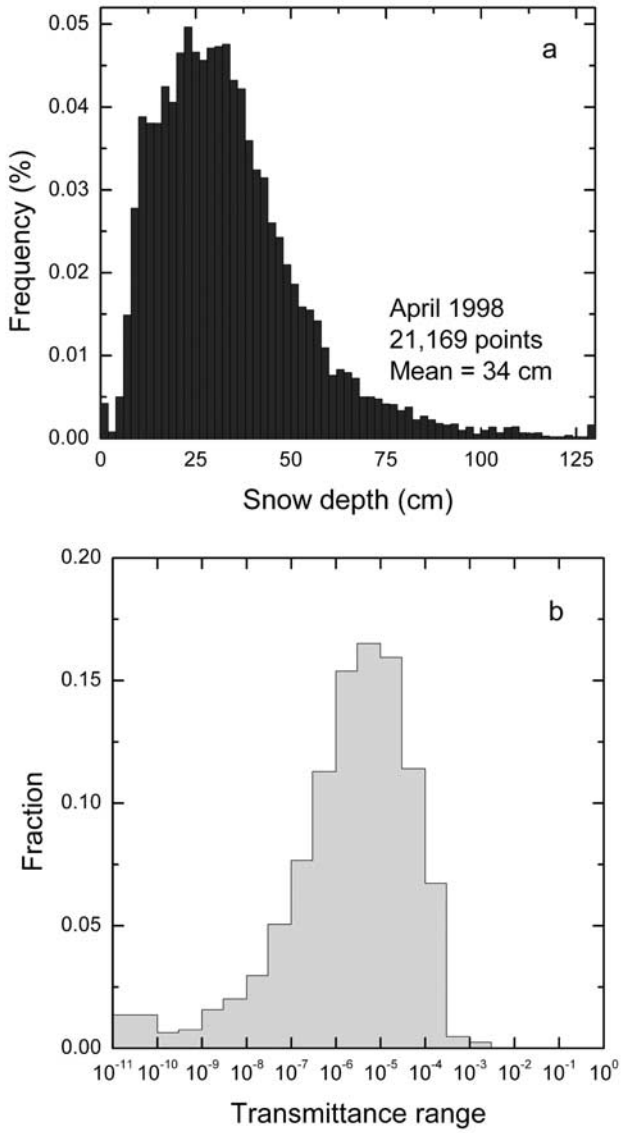

Figure 5. Snow depth and light transmittance: (a) spring snow depth distribution measured at SHEBA and (b) computed fraction of incident transmitted through the snow cover.

3.2. Transmittance

[19] Determining the aggregate transmittance is more complex than determining the aggregate albedo, as it is more difficult to measure and is dependent on snow depth and ice thickness. Because of this, aggregate transmittance was calculated using our radiative transfer model [*Perovich*, 1990] coupled with SHEBA observations of snow depth [*Sturm et al.*, 2002] and mass balance [*Perovich et al.*, 2003].

[20] Prior to the onset of melt, a prime attribute of the sea ice cover is the pervasive presence of snow. *Sturm et al.* [2002] examined in detail the spring snowpack at Ice Station SHEBA. The frequency distribution of snow depth determined from 21,000 measurements is presented in Figure 5a. The mean snow depth was 34 cm, and more

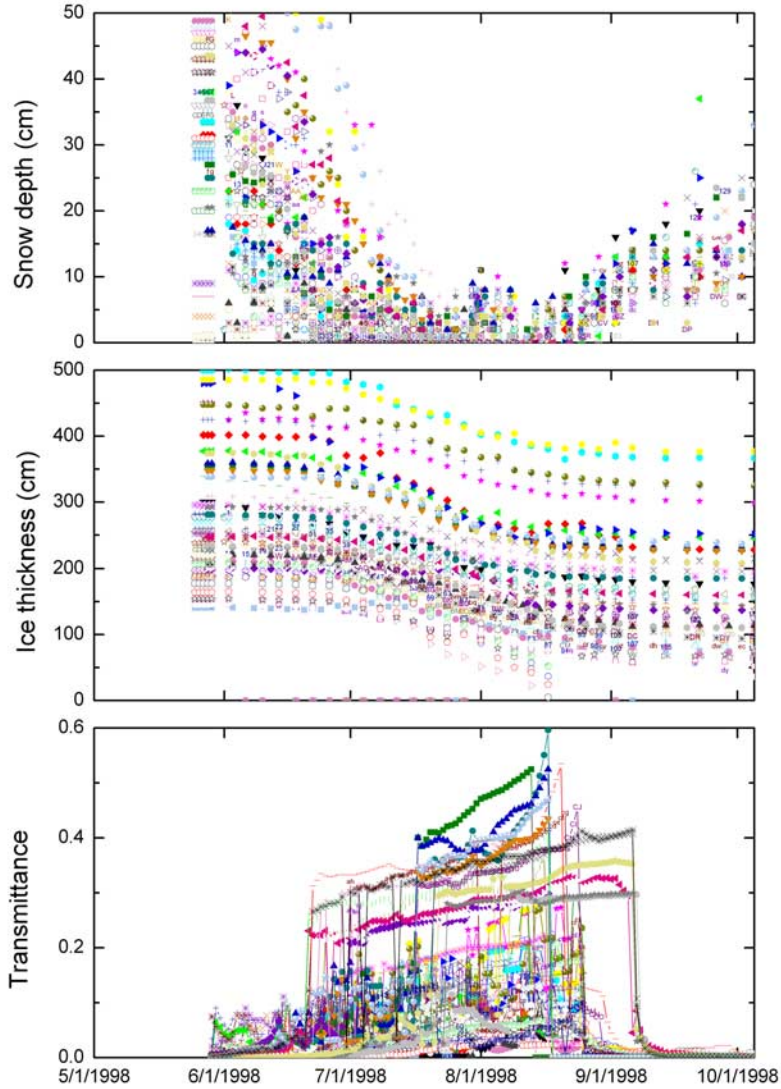

Figure 6. Time series from 80 mass balance sites of (a) snow depth or surface scattering layer thickness, (b) ice thickness [*Perovich et al.*, 2003], and (c) calculated transmittance.

importantly, from an optical perspective, over 99% of the ice is covered by an optically thick (5 cm) layer of snow. Figure 5b shows the distribution of light transmittance through the snow calculated using radiative transfer model and the snow depth distribution.

[21] Transmittance through the spring snow cover was quite small, averaging approximately 10^{-5}. Indeed, virtually all of the ice cover has snow transmittances less than 10^{-3}. Because of these small transmittance values, and for simplicity, it is assumed that prior to melt, no solar irradiance is transmitted through the snowpack. Errors in estimating transmittance associated with this assumption were less than 0.001. Therefore what is not reflected to the atmosphere is absorbed in the snow. Because the surface is a combination of snow-covered ice and open water, estimating transmittance is straightforward. Equation (2) reduces to simply $\overline{T} = (1 - \alpha_I)A_I = 0.93A_I$.

[22] Once melt begins, a more detailed approach is needed using observations from the thickness gauges and the radiative transfer model, as described in the approach. Figure 6 presents snow depths (Figure 6a) and ice thicknesses (Figure 6b) for the 80 thickness gauges used in the analysis. At all sites, there was a steady decline in snow depth during June. The depths of a few centimeters recorded during July and early August at most sites referred to the thickness of the surface scattering layer. The sites with 0-cm snow depth were melt ponds. Starting in mid-August, snow depths increased as fall freezeup began. Ice thicknesses (Figure 6b) decreased from June through September. The decrease averaged about 1.2 m and was most pronounced for melt pond and pressure ridge sites [*Perovich et al.*, 2003].

[23] The time series of transmittance for each gauge is displayed in Figure 6c. Transmittances ranged from 10^{-3} to 10^{-1} in early June as the snow cover melted. The melt pond curves are easily distinguished by their relatively large transmittances and their smooth temporal dependence. In general, pond transmittances monotonically increased during summer as the ice beneath the pond thinned. There was a sharp decrease in pond transmittance when the pond surface froze and became covered by snow. The smaller

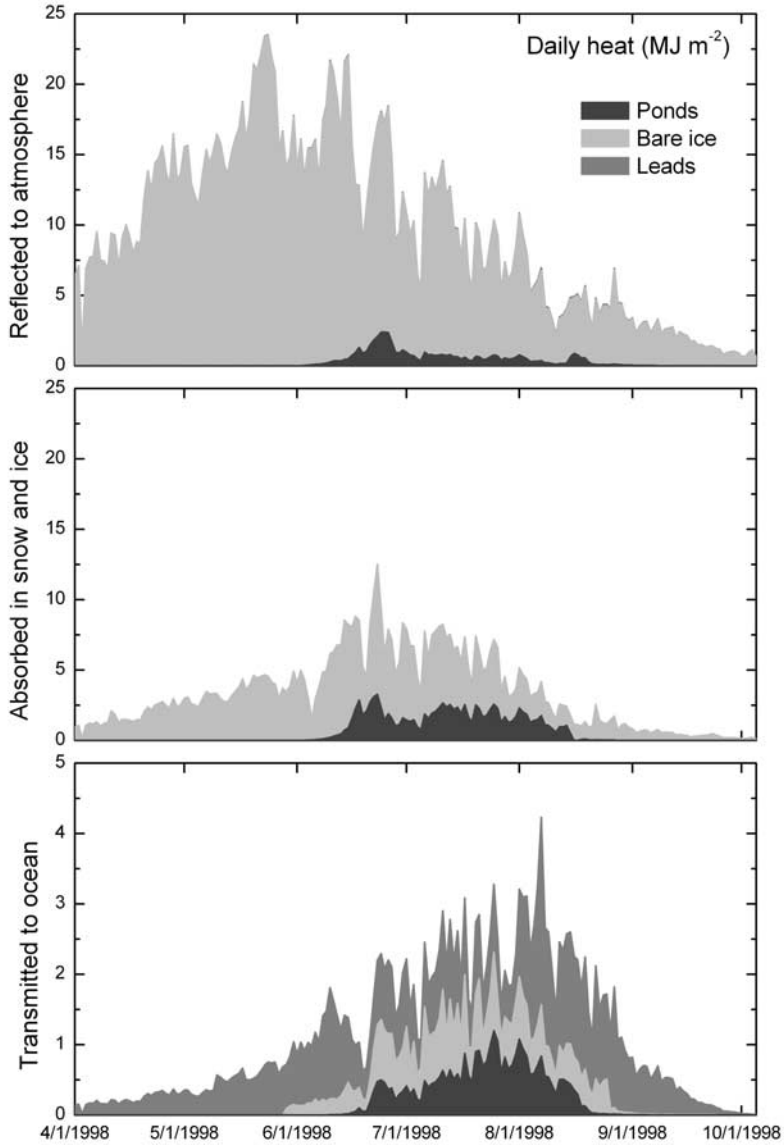

Figure 7. Time series of solar partitioning during SHEBA: (a) reflected to the atmosphere, (b) absorbed in the snow and ice, and (c) transmitted to the ocean. Contributions from leads, ponds, and bare and snow-covered ice are highlighted.

ponds began to freeze over in mid-August, while the larger ponds remained open until mid-September. Bare ice transmittances were smaller than pond transmittances, but tended to fluctuate more due to changes in the thickness of the surface scattering layer. The surface scattering layer tended to increase on sunny days when there was more penetrating solar energy and to thin on cloudy days. By mid-September, freezeup and new snow had reduced transmittances at all sites to less than 0.01.

[24] Equations (1) and (2) were evaluated by combining the observations and calculations presented in Figures 4, 5, and 6. The aggregate-scale fractional partitioning of solar radiation at SHEBA is presented in Figure 7, with the contributions from leads, ponds, and snow-covered/bare ice denoted. The fraction reflected to the atmosphere is the same as the albedo plotted in Figure 4d with the contributions from ice, ponds, and leads highlighted. Figure 7a demonstrates that snow-covered and bare ice are responsible for most of the energy reflected back to the atmosphere. Leads, with their combination of small albedo and area fraction, contribute very little to reflection, about 0.01 at most. Ponds contribute more than leads, but still only a small portion, less than 0.1.

[25] The fraction absorbed in the snow and ice (Figure 7b) was between 0.15 and 0.2 in April and May, when the surface is covered by highly reflecting snow. Once melt begins and the albedo decreases, the absorbed fraction increases to peak values of 0.3–0.4 from mid-June through the end of July. There are fluctuations throughout the summer that were inversely correlated with changes in albedo. For example, a light dusting of snow resulted in an increase in aggregate-scale albedo and a decrease in absorbed. From mid-June to mid-August, ponds made a substantial contribution to the energy absorbed in the ice

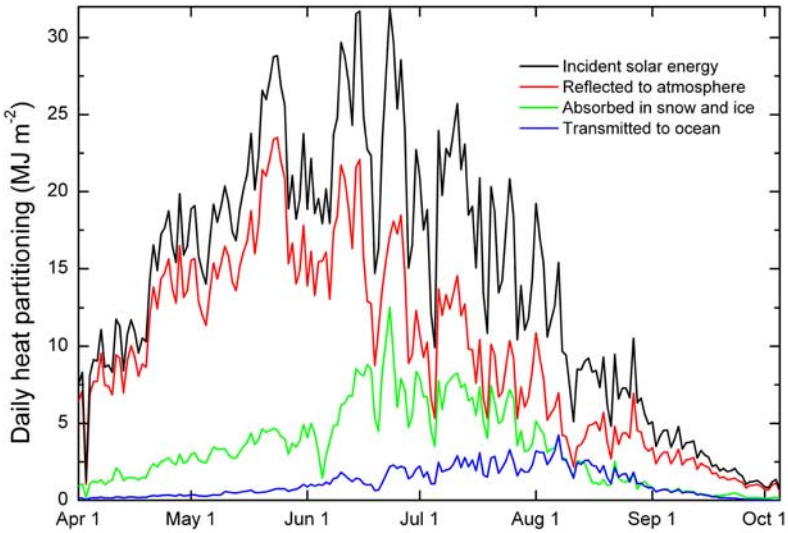

Figure 8. Time series solar daily partitioning of incident solar irradiance during SHEBA to reflection, absorption in the ice cover, and transmittance to the ocean.

cover. Even though ponds only covered about one fourth of the ice surface, they were responsible for one third to almost one half of the total solar energy absorbed, because their albedo was significantly less than that of bare ice. In early August, the ice pack diverged, decreasing the ice concentration and, consequently, the energy absorbed in the ice. Another major decrease occurred in mid-August, as the ponds began to freeze and snow fell and accumulated on the surface. This event caused a very sharp decrease of more than an order of magnitude in the pond contribution to absorbed energy.

[26] The time series of the fraction of the incident solar energy transmitted to the ocean is plotted in Figure 7c. Prior to melt, the transmitted fraction was quite small, as there was negligible transmittance through the snow-covered ice and leads only covered a few percent of the total ice cover. There was a slow, but steady, increase in transmittance in June and July, as the ice thinned and the melt ponds developed. The transmittance increased during the summer, reaching maximum values of 0.15–0.27 in August. At the beginning of August, the transmittance almost doubled as a direct result of the ice divergence that increased the open water fraction from 0.05 to 0.20. There were substantial contributions to transmittance from both ponded ice and bare ice. For example, during July, the transmittance contributions from leads, ponds, and bare ice were roughly comparable. This was surprising in light of earlier findings [*Maykut and McPhee*, 1995] that indicated that the source of ocean heat flux was solar radiation deposited in leads. This will be discussed in detail in the next section.

4. Discussion

[27] The seasonal cycle of daily solar energy input for SHEBA (Figure 8) was determined by combining the solar partitioning fractions with the time series of incident solar irradiance. The incident, reflected, absorbed, and transmitted all demonstrate a general seasonal cycle, but the timing of the cycle varies somewhat. The amount of energy reflected to the atmosphere was greatest in May, when both the surface albedo and the incident irradiance were large. Even though the incident solar irradiance increased to its peak value in June, the energy reflected to the atmosphere declined owing to the decrease in albedo. After June, the energy reflected to the atmosphere continued to decline as both the albedo and the incident irradiance decreased. The energy absorbed in the snow and ice increased slowly in April and May in conjunction with the increase in incident solar irradiance. There was a sharp increase in June associated with the onset of melt. The maximum daily value of energy absorbed in the snow and ice was 12.5 MJ m^{-2} on 23 June: enough energy to thin the ice by about 4 cm. The energy transmitted to the ocean increased slowly over the summer, reaching its maximum value near the end of the melt season in mid-August. At this time the incident irradiance was only two thirds of the peak June value. However, both the albedo and ice thickness were at minima and lead and pond fractions were at maxima, resulting in significant energy input to the ocean.

[28] The distribution of solar energy and the relative contributions from snow and ice, ponds, and leads are summarized in Table 1. The spatially and temporally averaged albedos were 0.82 during premelt, 0.60 during melt, and 0.66 in freezeup. The greatest solar energy input to the snow and ice was during the melt season, when the albedo was small and the incident solar energy was large. Ponds had a major impact in summer, but little influence during freezeup. In premelt and freezeup, virtually all of the solar energy input to the ocean came through leads. However, during the melt season, the combined contribution of solar energy transmitted through bare ice and ponds was equivalent to that through leads.

[29] The total solar incident solar energy at SHEBA from 1 April through 5 October 1998 was 2600 MJ m^{-2}. The incident solar radiation was partitioned with 68% reflected to the atmosphere, 24% absorbed in the snow and ice, and 8% transmitted to the ocean (Figure 9). These values are quite

Table 1. Partitioning of the Incident Solar Energy During Premelt, Melt, and Freezeup at SHEBA in 1998[a]

Period	Duration	Days	Incident Solar	Reflected to Atmosphere				Absorbed in Snow and Ice				Transmitted to Ocean			
				Total	Snow/ice	Ponds	Leads	Total	Snow/ice	Ponds	Leads	Total	Snow/ice	Ponds	Leads
Pr-melt	1 April to 29 May	59	963	788	786	0	2	154	154	0	0	22	0	0	22
Melt	30 May to 15 Aug.	78	1459	873	818	50	5	435	323	112	0	151	42	33	77
Freezeup	16 Aug. to 5 Oct.	50	205	135	128	4	2	34	34	1	0	36	5	1	30
Total	1 April to 5 Oct.	187	2627	1796	1732	54	9	623	511	112	0	208	47	34	128

[a]Units are MJ m^{-2}.

similar to the estimates of 69% reflected, 27% absorbed, and 4% transmitted calculated by *Ebert et al.* [1995]. The most notable difference is the factor of 2 increase in transmittance for the SHEBA analysis. This doubling is a direct consequence of the thinner ice at SHEBA.

[30] Figure 9 illustrates the relative contributions to this partitioning from snow and ice, ponds, and leads. Snow and bare ice dominated reflection back to the atmosphere, with ponds contributing only 3% and leads less than 1%. The total estimated solar energy absorbed in the ice cover was 623 MJ m^{-2}, with 82% in snow-covered or bare ice and the remaining 18% in ponds. This is enough energy to melt the entire snow cover (average depth and density of 0.34 m and 340 Mg m^{-3} [*Sturm et al.*, 2002]) plus 1.95 m of ice. By comparison, the mass balance measurements showed an average summer surface ablation of 0.64 m [*Perovich et al.*, 2003]. Of course, not all of the absorbed solar energy contributes directly to surface melting; some is absorbed deeper in the ice, where it causes internal melting [*Untersteiner*, 1961]. In addition, solar energy is not the only term in the surface heat budget. There are also contributions from longwave radiation and sensible and latent heat [*Persson et al.*, 2002]. These calculations do indicate that absorbed solar energy plays a major role in surface ablation.

[31] Much, but not all, of the solar energy transmitted to the ocean was through leads. Significant portions were also transmitted through bare ice (23%) and ponded ice (16%). The energy deposited in the ocean is of special interest because of its impact on the ocean heat flux (F_w). This component of the sea ice energy balance causes melting at the underside of the ice and retards freezing [*Untersteiner*, 1961; *Wettlaufer*, 1991; *Maykut and McPhee*, 1995; *Perovich and Elder*, 2002]. Analyzing results from the summer 1975 AIDJEX program conducted in the Beaufort Sea, *Maykut and McPhee* [1995] determined that the source of the ocean heat flux was solar energy deposited in leads (88%) and transmitted through ice less than 1.8 m thick (12%).

[32] The heat exchange from the ocean to the ice (Q_w) can be determined from measurements of ice temperature and bottom mass balance using the relationship

$$F_w \Delta t = Q_w = (Q_c + Q_s + Q_L), \quad (3)$$

where Δt is the time interval and Q_c, Q_s, and Q_L are the conductive, sensible, and latent heats in the ice [*McPhee and Untersteiner*, 1982]. The sign convention is that cooling, freezing, and upward heat flow are negative, while warming, melting, and downward heat flux are positive.

[33] Monthly averages of F_w for undeformed ice at SHEBA were only a few W m^{-2} in April and May, increasing to 10–20 W m^{-2} from June through August. The primary period of interest in this study is the summer, when the ice temperature is close to isothermal. During this time, $Q_c \sim Q_s \sim 0$ and equation (3) reduces to $F_w \Delta t = Q_L$. This does represent a lower bound on F_w, as there are small positive contributions from Q_c and Q_s in the spring. The latent heat source is melting at the bottom of the ice and

$$Q_L = \rho_i L_f \Delta H_i,$$

where ρ_i is the density of sea ice = 900 Mg m^{-3}, L_f is the latent heat of fusion = 335 kJ kg^{-1}, and ΔH_i is the change in ice thickness attributable to bottom melting.

[34] A time series of ΔH_i was derived by averaging bottom melt rates from 80 SHEBA thickness gauges [*Perovich et al.*, 2003]. As before, the critical assumption is that the thickness gauges provided a representative sample of the SHEBA region. The cumulative Q_L from April through early October is plotted in Figure 10. Also plotted is the cumulative heat input to the ocean from solar energy deposited through leads, bare ice, and melt ponds. The total amount of heat used for bottom melting was 183 MJ m^{-2}. The total energy transmitted through leads was only 127 MJ m^{-2}, only 70% of the energy used for melting. This is in sharp contrast to the findings from AIDJEX [*Maykut and McPhee*, 1995], where 88% of the bottom melting energy was transmitted through leads. During SHEBA the solar energy deposited in leads was

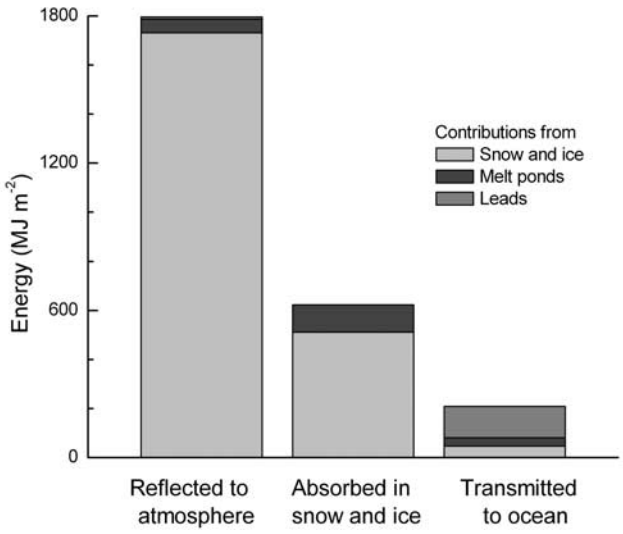

Figure 9. Partitioning of incident solar energy at SHEBA showing relative contributions from snow and ice, ponds, and leads to this partitioning.

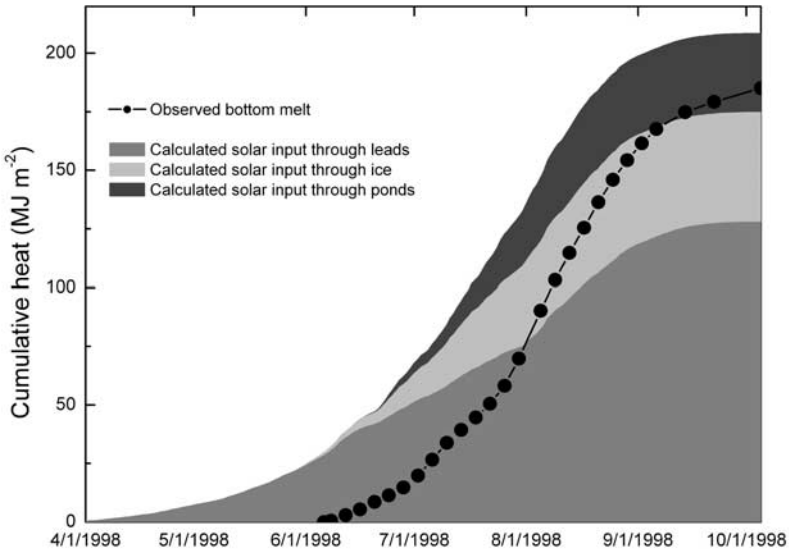

Figure 10. Time series of cumulative solar energy input to the ocean from leads, ice, and ponds and the cumulative heat needed for the observed SHEBA bottom ablation as determined from 80 thickness gauges [*Perovich et al.*, 2003].

insufficient to account for all of the ocean heat flux; substantial contributions from transmittance through bare ice (47 MJ m^{-2}) and melt ponds (34 MJ m^{-2}) were needed. The total heat input to the ocean was 208 MJ m^{-2}, 25 MJ m^{-2} more than was used in bottom melting. In all likelihood this additional solar energy was used in lateral melting of the ice floes.

[35] This marks a significant change in the interaction of solar energy with the sea ice cover. Compared to AIDJEX [*Maykut and McPhee*, 1995], substantial amounts of solar energy were transmitted to the ocean through the summer ice cover of SHEBA. This was a direct consequence of the thinner ice cover at SHEBA. Maykut and McPhee classified AIDJEX thin ice as less than 1.8 m. By the end of the SHEBA melt season, the mean thickness was 1.58 m and the median was 1.43 m and all of the unridged ice was less than 1.8 m thick. While bare ice albedos were the same for both experiments, the thinner ice at SHEBA resulted in smaller pond albedos and greater transmittance for both ponds and bare ice. Transmittance through the ice cover was over a third of the total input to the ocean at SHEBA, much greater than the 12% contribution during AIDJEX. The impact of enhanced solar transmission through thinner ice is evident in the total bottom ablation: 0.34 m during AIDJEX and 0.62 m in SHEBA.

[36] The thinner ice at SHEBA affected not only the magnitude of the solar energy partitioning, but its fundamental nature. Substantial amounts of solar radiation were transmitted through the melt season ice cover at SHEBA. The comparison between AIDJEX and SHEBA provides a starting point to speculate on potential changes in solar partitioning in a warming Arctic. For the bare ice observed at SHEBA (H_i > 1 m), the albedo was not influenced by changes in thickness, primarily because of the presence of the surface scattering layer. If there is a surface scattering layer, bare ice albedos, and consequently the magnitude of the bare ice component of solar input to the system, will remain unchanged. However, the input will be partitioned differently, with less absorbed in the ice and more transmitted to the ocean. Unlike the bare ice albedo, pond albedos are sensitive to the thickness of the underlying ice [*Perovich et al.*, 2002a, 2002b]. As the ice thins, pond albedos will decrease, enhancing the solar input to the system. Ponds will begin to melt through to the ocean, creating, in essence, mini-leads and greatly augmenting solar input to the ocean. In general, continued ice thinning will result in more solar energy input to the ice-ocean system and deeper energy input (i.e., ocean rather than ice). In a simplistic sense, the deeper the deposition of solar energy, the more difficult it is to extract. Deeper deposition will tend to accelerate the positive ice-albedo feedback.

[37] Observational and modeling work on light transmission through the ice cover would help refine estimates of solar partitioning. To fully explore partitioning in future sea ice scenarios, a greater understanding is needed of the optical and physical properties of ice less than 1 m thick. The greatest uncertainty concerns the fate of the bare ice surface scattering layer, if the ice cover continues to thin. We know that penetrating solar radiation and drainage of meltwater are needed for this layer to form. If the ice becomes too thin, and the freeboard too small, this 1- to 3-cm-thick-layer might disappear. The albedo would decrease from 0.65 to approximately 0.4, sharply increasing the solar input to the bare ice and to the ocean. For example, without the surface scattering layer at SHEBA, approximately an additional 250 MJ m^{-2} would have been input to the ice ocean system, enough energy to thin the ice by 0.85 m.

[38] **Acknowledgments.** The SHEBA program was sponsored by the National Science Foundation's Office of Polar Programs and the Office of Naval Research's High Latitude Physics Program. This work was funded under the Office of Naval Research Contract N0001402MP20065 and by the NASA contract NNHO4AA71L. The author thanks the SHEBA Logistics Office and the crew of the Canadian Coast Guard Icebreaker *Des Groseilliers* for their support during the field program, R.E. Moritz for

the incident solar radiation data, T. Grenfell, B. Light, J. Ukita, H. Eicken, and J. Richter-Menge for their assistance in making the summer mass balance and optical measurements, and C. Perovich for her assistance with the radiative transfer modeling.

References

Battisti, D. S., C. M. Bitz, and R. E. Moritz (1997), Do general circulation models underestimate the natural variability in the Arctic climate?, *J. Clim.*, *10*, 1909–1920.

Buckley, R. G., and H. J. Trodahl (1987), Thermally driven changes in the optical properties of sea ice, *Cold Reg. Sci. Technol.*, *14*, 201–204.

Comiso, J. C. (2002), A rapidly declining perennial sea ice cover in the Arctic, *Geophys. Res. Lett.*, *29*(20), 1956, doi:10.1029/2002GL015650.

Dickinson, R. E., G. A. Meehl, and W. M. Washington (1987), Ice-albedo feedback in a CO^2-doubling simulation, *Clim. Change*, *10*, 241–248.

Dunkle, R. V., and J. T. Bevans (1957), An approximate analysis of the solar reflectance and transmittance of a snow cover, *J. Meteorol.*, *13*, 212–216.

Ebert, E. E., J. L. Schramm, and J. A. Curry (1995), Disposition of solar radiation in sea ice and the upper ocean, *J. Geophys. Res.*, *100*, 15,965–15,975.

Grenfell, T. C. (1979), The effects of ice thickness on the exchange of solar radiation over the polar oceans, *J. Glaciol.*, *22*, 305–320.

Grenfell, T. C. (1983), A theoretical model of the optical properties of sea ice in the visible and near infrared, *J. Geophys. Res.*, *88*, 9723–9735.

Grenfell, T. C. (1991), Radiative transfer model for sea ice with vertical structure variations, *J. Geophys. Res.*, *96*, 16,991–17,001.

Grenfell, T. C., and G. A. Maykut (1977), The optical properties of ice and snow in the Arctic Basin, *J. Glaciol.*, *18*, 445–463.

Grenfell, T. C., and D. K. Perovich (1984), Spectral albedos of sea ice and incident solar irradiance in the Southern Beaufort Sea, *J. Geophys. Res.*, *89*, 3573–3580.

Hanesiak, J. M., D. G. Barber, R. A. De Abreu, and J. J. Yackel (2001), Local and regional albedo observations of Arctic first-year sea ice during melt ponding, *J Geophys. Res.*, *106*, 1005–1016.

Jin, Z., K. Stamnes, and W. F. Weeks (1994), The effect of sea ice on the solar energy budget in the atmosphere-sea ice-ocean system: A model study, *J. Geophys. Res.*, *99*, 25,281–25,294.

Johannessen, O. M., E. V. Shalina, and M. W. Miles (1999), Satellite evidence for an Arctic sea ice cover in transformation, *Science*, *286*(5446), 1937–1939.

Langleben, M. P. (1971), Albedo of melting sea ice in the southern Beaufort Sea, *J. Glaciol.*, *10*, 101–104.

Light, B., G. A. Maykut, and T. C. Grenfell (2003), A two-dimensional Monte Carlo model of radiative transfer in sea ice, *J. Geophys. Res.*, *108*(C7), 3219, doi:10.1029/2002JC001513.

Lynch, A. H., J. A. Maslanik, and W. Wu (2001), Mechanisms in the development of anomalous sea ice extent in the western Arctic: A case study, *J. Geophys. Res.*, *106*, 28,097–28,105.

Maykut, G. A., and M. G. McPhee (1995), Solar heating of the Arctic mixed layer, *J. Geophys. Res.*, *100*, 24,691–24,703.

McPhee, M. G., and N. Untersteiner (1982), Using sea ice to measure vertical heat flux in the ocean, *J. Geophys. Res.*, *87*, 2071–2074.

Moritz, R. E., J. A. Curry, A. S. Thorndike, and N. Untersteiner (1993), SHEBA, a research program on the surface heat budget of the Arctic Ocean, *Arct. Syst. Sci Rep. 3*, 34 pp., Natl. Sci. Found., Washington, D. C.

Parkinson, C. L., and D. J. Cavalieri (2002), A 21 year record of Arctic sea-ice extents and their regional, seasonal and monthly variability and trends, *Ann. Glaciol.*, *34*, 441–446.

Parkinson, C. L., D. J. Cavalieri, P. Gloersen, H. J. Zwally, and J. C. Comiso (1999), Arctic sea ice extents, areas, and trends, 1978–1996, *J. Geophys. Res.*, *104*(C9), 20,837–20,856.

Pegau, W. S., and C. A. Paulson (2001), The albedo of Arctic leads in summer, *Ann. Glaciol.*, *33*, 221–224.

Perovich, D. K. (1990), Theoretical estimates of light reflection and transmission by spatially complex and temporally varying sea ice covers, *J. Geophys. Res.*, *95*, 9557–9567.

Perovich, D. K. (1996), The optical properties of sea ice, *Monogr. 96-1*, 25 pp., Cold Reg. Res. and Eng. Lab., Hanover, N. H.

Perovich, D. K., and B. Elder (2002), Estimates of ocean heat flux during SHEBA, *Geophys. Res. Lett.*, *29*(9), 1344, doi:10.1029/2001GL014171.

Perovich, D. K., C. S. Roesler, and W. S. Pegau (1998), Variability in sea ice optical properties, *J. Geophys. Res.*, *103*, 1193–1209.

Perovich, D. K., et al. (1999a), Year on ice gives climate insights, *EOS Trans. AGU*, *80*(481), 485–486.

Perovich, D. K., T. C. Grenfell, B. Light, J. A. Richter-Menge, M. Sturm, W. B. Tucker III, H. Eicken, G. A. Maykut, and B. Elder (1999b), *SHEBA: Snow and Ice Studies* [CD-ROM], Cold Reg. Res. and Eng. Lab., Hanover, N. H.

Perovich, D. K., T. C. Grenfell, B. Light, and P. V. Hobbs (2002a), The seasonal evolution of Arctic sea ice albedo, *J. Geophys. Res.*, *107*(C10), 8044, doi:10.1029/2000JC000438.

Perovich, D. K., W. B. Tucker III, and K. A. Ligett (2002b), Aerial observations of the evolution of ice surface conditions during summer, *J. Geophys. Res.*, *107*(C10), 8048, doi:10.1029/2000JC000449.

Perovich, D. K., T. C. Grenfell, J. A. Richter-Menge, B. Light, W. B. Tucker III, and H. Eicken (2003), Thin and thinner: Ice mass balance measurements during SHEBA, *J. Geophys. Res.*, *108*(C3), 8050, doi:10.1029/2001JC001079.

Persson, P. O. G., C. W. Fairall, E. Andreas, P. Guest, and D. K. Perovich (2002), Measurements near the atmospheric surface flux group tower at SHEBA: Near-surface conditions and surface energy budget, accepted, *J. Geophys. Res.*, *107*(C10), 8045, doi:10.1029/2000JC000705.

Radionov, V. F., N. N. Bryazgin, and E. I. Alexandrov (1997), The snow cover of the Arctic Basin, *Tech. Rep. 9701*, App. Phys. Lab., Univ. of Wash., Seattle.

Richter-Menge, J. A., and D. K. Perovich (2001), The impact of summer ice dynamics on the surface heat budget of the Arctic Ocean, *Ann. Glaciol.*, *33*, 201–206.

Rind, D., R. Healy, C. Parkinson, and D. Martinson (1995), The role of sea ice in $2 \times CO_2$ climate model sensitivity: I. The total influence of sea ice thickness and extent, *J. Clim.*, *8*, 450–463.

Rothrock, D. A., Y. Yu, and G. A. Maykut (1999), Thinning of the Arctic sea ice cover, *Geophys. Res. Lett.*, *26*(23), 3469–3472.

Serreze, M. C., J. E. Walsh, F. S. Chapin, T. Osterkamp, M. Dyurgerov, V. Romanovsky, W. C. Oechel, J. Morison, T. Zhang, and R. G. Barry (2000), Observational evidence or recent change in the northern high-latitude environment, *Clim. Change*, *46*, 159–207.

Serreze, M. C., J. A. Maslanik, T. A. Scambos, F. Fetterer, J. Stroeve, K. Knowles, C. Fowler, S. Drobot, R. G. Barry, and T. M. Haran (2003), A record minimum arctic sea ice extent and area in 2002, *Geophys. Res. Lett.*, *30*(3), 1110, doi:10.1029/2002GL016406.

Smith, R. C., and K. S. Baker (1981), Optical properties of the clearest natural waters (200–800 nm), *Appl. Opt.*, *20*, 177–184.

Sturm, M., J. Holmgren, and D. Perovich (2002), The winter snow cover on the sea ice of the Arctic Ocean at SHEBA: Temporal evolution and spatial variability, *J. Geophys. Res.*, *107*(C10), 8047, doi:10.1029/2000JC000400.

Tucker, W. B., III, J. W. Weatherly, D. T. Eppler, L. D. Farmer, and D. L. Bentley (2001), Evidence for rapid thinning of sea ice in the western Arctic Ocean at the end of the 1980s, *Geophys. Res. Lett.*, *28*(14), 2851–2854.

Untersteiner, N. (1961), On the mass and heat budget of Arctic sea ice, *Arch. Meteorol. Geophys. Bioklimatol., Ser. A*, *12*, 151–182.

Uttal, T., et al. (2002), Surface heat budget of the Arctic Ocean, *Bull. Am. Meteorol. Soc.*, *83*, 255–275.

Vinnikov, K. Y., A. Robock, R. J. Stouffer, J. E. Walsh, C. L. Parkinson, D. J. Cavalieri, J. F. B. Mitchell, D. Garrett, and V. F. Zakharov (1999), Global warming and Northern Hemisphere sea ice extent, *Science*, *286*(5446), 1934–1937.

Voss, K. J., and J. S. Schoonmaker (1992), Temperature dependence of beam scattering in young sea ice, *Appl. Opt.*, *31*, 3388–3389.

Wettlaufer, J. S. (1991), Heat flux at the ice-ocean interface, *J. Geophys. Res.*, *96*, 7215–7236.

D. K. Perovich, Engineer Research and Development Center, Cold Regions Research and Engineering Laboratory, 72 Lyme Road, Hanover NH 03755, USA. (donald.k.perovich@erdc.usace.army.mil)